Entropic Effects on the Dynamical Bottleneck Location and Tunneling Contributions for $C_2H_4 + H \rightarrow C_2H_5$: Variable Scaling of External Correlation Energy for Association Reactions

Jordi Villà,[†] Angels González-Lafont,[†] José M. Lluch,*[,†] and Donald G. Truhlar*[,‡]

Contribution from the Departament de Química, Universitat Autònoma de Barcelona, 08193-Bellaterra, Barcelona, Spain, and Department of Chemistry and Supercomputer Institute, University of Minnesota, Minneapolis, Minnesota 55455-0431

Received January 12, 1998

Abstract: The temperature dependence of the dynamical bottleneck location for the prototype olefin addition process $H + C_2H_4$ has been studied by variational transition state theory. In addition, a multidimensional tunneling calculation has been carried out. To obtain a reliable potential energy profile, a new way to extrapolate electronic structure calculations to the limit of full configuration mixing and a complete electronic basis set is proposed. The method, called variable scaling of external correlation (VSEC) uses a scale factor that varies with geometry to combine a complete-active-space self-consistent-field (CASSCF) calculation with a calculation including an appreciable amount of the dynamical correlation energy. The parameters in the scaling factor are adjusted to experimental or high-quality theoretical data at critical points. For the title reaction we find excellent agreement with experiment at all temperatures both for the rate constant of the association reaction and also for the rate constant of its reverse dissociation, and we use the resulting model to infer critical details of the dynamics. In particular, we find that dynamical bottlenecks are ∼0.06−0.15 Å tighter than the saddle point, with bending frequencies 1.2−1.8 times higher than at the saddle point. Furthermore, we conclude that tunneling effects account quantitatively for the curvature of the Arrhenius plots.

Introduction

The addition of a free radical to an olefin to form an alkyl radical is a prototype class of association reactions. The simplest of these reactions is addition of a hydrogen atom to ethylene, which is of great fundamental and applied importance. For example, it is the simplest reaction involving addition to a double bond, and the reaction and its reverse are critical steps in the industrially important pyrolysis (cracking) of ethane feedstock,[1,2] which is a major source of ethylene. The reverse reaction is also important in low-temperature combustion, where it competes with the oxidation of ethyl radical.[2] This reaction has been extensively studied both experimentally[1−21] and theoretically,[22−32] but is still not completely understood. Overall rate constants for both association and dissociation (k_a and k_d, respectively) have been reported in the literature, including their pressure dependence and the temperature dependence of their high-pressure values. We consider the well-known mechanism

[†] Departament de Química.

[‡] Department of Chemistry and Supercomputer Institute.

(1) Pilling, M. J. In *Modern Gas Kinetics*; Pilling, M. J., Smith, I. W. M., Eds.; Blackwell Scientific: Oxford, 1987; p 330.

(2) Davies, J. W.; Pilling, M. J. *Adv. Gas-Phase Photochem. Kinet*. **1989**, *2*, 105.

(3) (a) Lin, M. C.; Back, M. H. *Can. J. Chem*. **1996**, *44*, 505. (b) Lin, M. C.; Back, M. H. *Can. J. Chem*. **1966**, *44*, 505. (c) Loucks, L. F.; Laidler, K. J. *Can. J. Chem*. **1967**, *45*, 2795.

(4) Braun, W.; Lenzi, M. *Discuss. Faraday Soc*. **1967**, *44*, 252.

(5) Westenberg, A. A.; deHaas, N. *J. Chem. Phys*. **1969**, *50*, 707.

(6) Kurylo, M. J.; Peterson, N. C.; Braun, W. *J. Chem. Phys*. **1970**, *53*, 2776.

(7) Eyre, J. A.; Hikida, T.; Dorfman, L. *J. Chem. Phys*. **1970**, *53*, 1281.

(8) Barker, J. R.; Keil, D. G.; Michael, J. V.; Osborne, D. T. *J. Chem. Phys*. **1970**, *52*, 2079.

(9) (a) Michael, J. V.; Cowfer, J. A.; Keil, D. G.; Yeh, C. *J. Phys. Chem*. **1971**, *75*, 1584. (b) Cowfer, J. A.; Michael, J. V. *J. Chem. Phys*. **1975**, *62*, 3504.

(10) (a) Michael, J. V.; Osborne, D. T.; Suess, G. N. *J. Chem. Phys.* **1973**, *58*, 2300. (b) Jones, W. E.; Macknight, S. D.; Teng, L. *Chem. Rev*. **1973**, *73*, 407.

(11) Lee, J. H.; Michael, J. V.; Payne, W. A.; Stief, L. J. *J. Chem. Phys*. **1978**, *68*, 1817.

(12) Oka, K.; Cvetanović, R. J. *Can. J. Chem*. **1979**, *57*, 777.

(13) Pacey, P. D.; Wimalasena, J. H. *Chem. Phys. Lett*. **1980**, *76*, 433.

(14) (a) Sugawara, K.; Okazaki, K.; Sato, S. *Chem. Phys. Lett*. **1981**, *78*, 259. (b) Sugawara, K.; Okazaki, K.; Sato, S. *Bull. Chem. Soc. Jpn.* **1981**, *54*, 2872.

(15) Pacey, P. D.; Wimalasena, J. H. *J. Phys. Chem*. **1984**, *88*, 5657.

(16) Trenwith, A. B. *J. Chem. Soc., Faraday Trans*. **1986**, *82*, 457.

(17) Lightfoot, P. D.; Pilling, M. J. *J. Phys. Chem*. **1987**, *91*, 3373.

(18) Simon, Y.; Foucaut, J. F.; Scacchi, G. *Can. J. Chem*. **1988**, *66*, 2142.

(19) Garner, D. M.; Fleming, D. G.; Arseneau, D. J.; Senba, M.; Reid, I. D.; Mikula, R. J. *J. Chem. Phys*. **1990**, *93*, 1732.

(20) Hanning-Lee, M. A.; Green, N. J. B.; Pilling, M. J.; Robertson, S. H. *J. Phys. Chem*. **1993**, *97*, 860.

(21) Feng, Y.; Niiranen, J. T.; Bencsura, Á.; Knyazev, V. D.; Gutman, D.; Tsang, W. *J. Phys. Chem*. **1993**, *97*, 871.

(22) Michael, J. V.; Suess, G. N. *J. Chem. Phys*. **1973**, *58*, 2807.

(23) (a) Sloane, C.; Hase, W. L. *Faraday Discuss. Chem. Soc*. **1977**, *62*, 210. (b) Hase, W. L.; Mrowka, G.; Brudzynski, R.; Sloane, C. S. *J. Chem. Phys*. **1978**, 69, 3548. (c) Hase, W. L.; Wolf, R. J.; Sloane, C. S. *J. Chem. Phys*. **1979**, *71*, 2911. (d) Hase, W. L.; Mrowka, G.; Brudzynski, R.; Sloane, C. S. *J. Chem. Phys*. **1980**, *72*, 6321.

(24) (a) Hase, W. L.; Ludlow, D. M.; Wolf, R. J.; Schlick, T. *J. Phys. Chem*. **1981**, *85*, 958. (b) Schlegel, H. B. *J. Phys. Chem*. **1982**, *85*, 4878. (c) Hase, W. L.; Buckowski, D. G. *J. Comput. Chem*. **1982**, *3*, 335.

(25) Hase, W. L.; Schlegel, H. B. *J. Phys. Chem*. **1982**, *86*, 3901.

(26) Schlegel, H. B.; Bhalla, K. C.; Hase, W. L. *J. Phys. Chem*. **1982**, *86*, 4883.

(27) (a) Hase, W. L.; Buckowski, D. G.; Swamy, K. N. *J. Phys. Chem*. **1983**, *87*, 2754. (b) Swamy, K. N.; Hase, W. L. *J. Phys. Chem*. **1983**, *87*, 4715.

S0002-7863(98)00131-0 CCC: $15.00
Published on Web 05/22/1998

$$H + C_2H_4 \rightleftarrows C_2H_5^* \quad (1)$$

$$C_2H_5^* + M \rightleftarrows C_2H_5 + M \quad (2)$$

where the asterisk indicates vibrational and rotational excitation. The high-pressure association is of special interest because it corresponds to the rate constant for the elementary step (1), and the high-pressure dissociation is of special interest because Rice−Ramsperger−Kassel−Marcus (RRKM) theory reduces to transition state theory in the high-pressure limit. High-pressure rate constants k_a^∞ and k_d^∞ have been measured in the ranges 198−800 K[4,6−9,11,12,17,20] and 673−913 K, respectively.[3,15,16,18,21] Recently, Feng et al.[21] developed an RRKM transition state model, based on previous experimental data in the range 198−800 K, for extrapolating k_a^∞ up to 1100 K. The model leads to the following recommended rate expression for k_a^∞:

$$k_a^\infty(T) = 1.795 \times 10^{-12} T^{0.454} \exp(-917/T) \text{ cm}^3 \text{ mol}^{-1} \text{ s}^{-1} \quad (3)$$

Values obtained from eq 3 by the same authors, when used together with thermodynamic properties of C_2H_5, yield a new recommended expression of the high-pressure dissociation rate constant in the same temperature range, 198−1100 K:

$$k_d^\infty(T) = 1.11 \times 10^{10} T^{1.037} \exp(-18504/T) \text{ s}^{-1} \quad (4)$$

Feng et al.[21] used k_d^∞ values from eq 4 to test agreement of their theoretical results with experiment in the 673−913 K range and to interpret their experimental results near the low-pressure limit from 875 to 1094 K.

In addition to these experimental results and experimentally based models, several theoretical studies of the association and dissociation reactions have been carried out.[22−32] A major subject of discussion has been the question of whether transition state and RRKM theory can simultaneously fit the rates of the C_2H_4 + H addition and the C_2H_5 unimolecular dissociation. Considerable progress was reported in 1982 by Hase and Schlegel,[25,26] who proposed a loose transition state model based on ab initio calculations of the geometry and vibrational frequencies for the transition state. Their model appeared to give an acceptable fit to available experimental data. However, in the aforementioned study by Feng et al.,[21] it was concluded that a tighter transition state than that used by Hase and Schlegel is required for a good fit to the temperature dependence of the experimental k_d^∞. In view of this finding, Hase et al.[29] reassessed the kinetics of the C_2H_4 + H $\rightleftarrows$ C_2H_5 system, and they tried to use high-level ab initio calculations to develop a definitive transition state model that fits the most reliable experimental results. The main conclusions of this new work are that it is very difficult to obtain quantitative ab initio predictions of the energetics for this reaction (so the forward barrier height was taken as an adjustable parameter in fitting the experimental rates, and it was combined with the enthalpy of reaction proposed in previous work[20] for the best estimate of the reverse barrier), and that the loose model proposed in the earlier paper[25] is good enough to describe the geometry and frequencies for the transition state. With regard to the former conclusion, we note that several other studies have also shown the difficulty of calculating the barrier heights of radical addition reactions (see, for example, refs 31−37). One of the aims of the present work is to find a reliable method to evaluate enough of the potential energy surface to perform more sophisticated dynamics calculations than have been carried out so far. In this regard, we note that Hase et al.[29] used conventional transition state theory; that is, the transition state position was assumed to be fixed at the saddle point structure. In this way, the same loose transition state model was used for the entire range of temperatures studied. One justification for this is an early study[38] in which the 0 K variational transition state was found to be close to the saddle point. We believe though that more definitive studies including finite-temperature dynamical bottlenecks are required to answer this question because entropic effects on the location of the dynamical bottleneck should be considered whenever the intrinsic barrier is small and the potential is relatively flat in its vicinity.[39]

One objective in this work is to reexamine the addition and unimolecular dissociation rate constants under the more flexible assumption that the location of the transition state along the reaction path is optimized by variational transition state theory. This reexamination will allow more definitive conclusions about the looseness or tightness of the transition state as a function of temperature as well as answer the question of whether the dynamical bottleneck location is temperature dependent. A second goal is to carry out a multidimensional tunneling calculation. To accomplish these objectives we use a new method presented here called variable scaling of external correlation energy.

Methods and Calculations

Geometries, energies, and first and second energy derivatives were calculated using the Gaussian94 system of programs.[40] We recall the general notation X//Y[41] to denote geometry optimization and Hessian evaluation (for frequencies) at level Y followed by a single-point energy calculation at level X. As usual, we omit //Y if Y is the same as X. A consequence of this standard notation is that X//Y calculations involve a level-Y Hessian, whereas X calculations involve a level-X Hessian.[42] As usual, X and Y each have the form L/B, where L denotes the Hartree−Fock or correlation level, and B denotes the one-electron basis set.

Stationary point geometries (reactants, product, and saddle point) were optimized, and the harmonic vibrational frequencies were calculated using the 6-31G(*d*,*p*) basis set[41] (called B1 in this work) at two levels: Hartree−Fock[41] (HF) and Møller−

(28) Sosa, C.; Schlegel, H. B. *Int. J. Quantum Chem.* **1986**, *29*, 1001.
(29) Hase, W. L.; Schlegel, H. B.; Balbyshev, V.; Page, M. *J. Phys. Chem.* **1996**, *100*, 5354; **1997**, *101*, 5026(E).
(30) Mole, S. J.; Zhou, X.; Liu, R. *J. Phys. Chem.* **1996**, *100*, 14665.
(31) Nguyen, M. T.; Creve, S.; Vanquickenborne, L. G. *J. Phys. Chem.* **1996**, *100*, 18422.
(32) Jursic, B. S. *J. Chem. Soc., Perkin Trans. 2* **1997**, *637*.
(33) Barone, V.; Orlandini, L. *Chem. Phys. Lett.* **1995**, *246*, 45.
(34) Villà, J.; González-Lafont, A.; Lluch, J. M.; Corchado, J. C.; Espinosa-García, J. *J. Chem. Phys.* **1997**, *107*, 7266.
(35) Schlegel, H. B. *J. Chem. Phys.* **1986**, *84*, 4530.
(36) Gonzalez, C.; Sosa, C.; Schlegel, H. B. *J. Phys. Chem.* **1989**, *93*, 2435, 8388(E).
(37) Wong, M.; Radom, L. *J. Phys. Chem.* **1995**, *99*, 8582.
(38) Hase, W. L. *Acc. Chem. Res.* **1983**, *16*, 258.
(39) (a) Garrett B. C.; Truhlar, D. G. *J. Am. Chem. Soc.* **1979**, *101*, 4534. (b) Garrett, B. C.; Truhlar, D. G. *J. Am. Chem. Soc.* **1979**, *101*, 5207.
(40) Frisch, M. J.; Trucks, G. W.; Schlegel, H. B.; Gill, P. M. W.; Johnson, B. G.; Robb, M. A.; Cheeseman, J. R.; Keith, T. A.; Petersson, G. A.; Montgomery, J. A.; Raghavachari, K.; Al-Laham, M. A.; Zakrzewski, V. G.; Ortiz, J. V.; Foresman, J. B.; Cioslowski, J.; Stefanov, B. B.; Nanayakkara, A.; Challacombe, M.; Peng, C. Y.; Ayala, P. Y.; Chen, W.; Wong, M. W.; Andres, J. L.; Replogle, E. S.; Gomperts, R.; Martin, R. L.; Fox, D. J.; Binkley, J. S.; Defrees, D. J.; Baker, J.; Stewart, J. P.; Head-Gordon, M.; Gonzalez, C.; Pople, J. A. *Gaussian94*; Gaussian, Inc.; Pittsburgh, PA, 1995.
(41) Hehre, W. J.; Radom, L.; Schleyer, P. v. R.; Pople, J. A. *Ab Initio Molecular Orbital Theory*; Wiley: New York, 1986.

Plesset second-order perturbation theory[41,43] (MP2). These geometries were also optimized with the 6-311G(*d*,*p*) basis set[41] (called B2) at four levels: HF, MP2, complete active space multiconfiguration SCF[44] (CASSCF), and quadratic configuration interaction with single and double excitations and a perturbative estimate of the effect of triple excitations[45] [QCISD(T)]. For the CASSCF calculations we used the same active space (three electrons distributed among three orbitals) as used by Hase et al.[29]

Starting from the MP2/B1 saddle point geometry we have calculated the minimum energy path[46,47] (MEP) and the potential energy along the minimum energy path, $V_{MEP}(s)$, where s denotes the distance along the MEP in an isoinertial mass-weighted or mass-scaled coordinate system,[46−50] by following the Gonzalez−Schlegel mass-weighted internal-coordinates reaction-path algorithm[51] at the MP2/Bl level. Note that although this algorithm carries out the calculation in internal coordinates, it does correctly yield the true MEP[46,47] through isoinertial coordinates. A gradient step size, δs, of 0.0319 Å (in mass-scaled coordinates with the scaling mass equal to 1 amu) was used to follow the MEP. For 22 points along this MEP (reactants, product, saddle point, and 19 nonstationary points with values of s from −0.083 to 0.344 Å, which correspond to R_1 distances between 1.793 and 2.171 Å) we have also calculated the force constant matrix at the same MP2/B1 level. Then, a generalized normal-mode analysis was performed in rectilinear[46,48−50,52,53] coordinates, which allows us to calculate both the vibrational partition function along the MEP and the vibrationally adiabatic potential energy curve[46,49,50,53−59]

$$V_a^G(s) = V_{MEP}(s) + \epsilon_{tran}^G(s) \qquad (5)$$

where $\epsilon_{tran}^G(s)$ is the zero-point energy (ZPE) at s from the generalized normal-mode vibrations transverse to the reaction path. Use of the reoriented dividing-surface (RODS) algorithm[60] to improve these generalized frequencies does not produce any significant change in the $V_a^G(s)$ curve, which indicates that the relatively large step size used to follow the MEP was accurate enough for this reaction. The use of curvilinear coordinates[61,62] was also explored, but they did not lead to significant improvement in the important range of s, so all results presented here were obtained with rectilinear coordinates.

For the aforementioned 22 points, we have also made single-point calculations at the two highest levels used in this work, obtaining improved values of $V_{MEP}(s)$ at the CASSCF(3,3)/B2//MP2/B1/// and QCISD(T)/B2//MP2/B1/// levels. (The X//Y notation indicates single-point energies by level X for geometries obtained at level Y, and X//Y/// indicates[42] single-point energy calculations at level X that are performed all along the MEP calculated at level Y, not just at the stationary points). It will be seen later that the energy of the maximum energy structure at the QCISD(T)/B2//MP2/B1/// level is very similar to the energy of the saddle point fully optimized at the QCISD(T)/B2 level. In addition, at the stationary points we carried out PMP2/B1//MP2/B1 calculations, where PMP2 denotes the spin-projected MP2 method:[36] this correction could be important because unrestricted Møller−Plesset perturbation theory suffers from serious spin contamination problems for radical addition reactions to ethylene.[28,33,34]

Rate constants were calculated by direct multidimensional semiclassical dynamics, i.e., including multidimensional quantum effects on the nuclear motion, by a semiclassical method, and by obtaining all required information about the potential energy surface directly from electronic structure calculations without the intermediacy of an analytic potential energy function.[63] Canonical variational transition state theory (CVT) rate constants[39,48−50,53,59,64] and semiclassical transmission coefficients[50,53,59,64] for addition and unimolecular dissociation reactions were calculated using a modified version of version 7.0 of the POLYRATE computer program[65−67] that includes the RODS algorithm already mentioned. Bound vibrational and rotational motions were assumed to be separable, and the vibrational partition functions were computed quantum mechanically within the harmonic approximation, except for the torsion around the C−C bond, which is considered a hindered rotor[68,69] in the generalized transition states and C_2H_5 product.

(42) Corchado, J. C.; Espinosa-García, J.; Hu, W.-P.; Rossi, I.; Truhlar, D. G. *J. Phys. Chem.* **1995**, *99*, 687.
(43) Møller, C.; Plesset, M. S. *Phys. Rev.* **1934**, *46*, 618.
(44) Roos, B. O.; Taylor, P. R.; Siegbahn, P. E. M. *Chem. Phys.* **1980**, *48*, 152.
(45) Pople, J. A.; Head-Gordon, M.; Raghavachari, K. *J. Chem. Phys.* **1987**, *87*, 5968.
(46) Truhlar, D. G.; Kuppermann, A. J. *J. Am. Chem. Soc.* **1971**, *93*, 1840.
(47) Fukui, K. *Pure Appl. Chem.* **1982**, *54*, 1825.
(48) Garrett, B. C.; Truhlar, D. G. *J. Chem. Phys.* **1979**, *70*, 1593.
(49) Garrett, B. C.; Truhlar, D. G. *J. Phys. Chem.* **1979**, *83*, 1079.
(50) Isaacson A. D.; Truhlar, D. G. *J. Chem. Phys.* **1982**, *76*, 1380.
(51) Gonzalez, C.; Schlegel, H. B. *J. Phys. Chem.* **1990**, *94*, 5523.
(52) Miller, W. H.; Handy, N. C.; Adams, J. E. *J. Chem. Phys.* **1980**, *72*, 99.
(53) Truhlar, D. G.; Isaacson, A. D.; Garrett, B. C. In *Theory of Chemical Reaction Dynamics*; Baer, M., Ed.; CRC: Boca Raton, FL, 1985; Vol. 4, p 65.
(54) Elaison, M. A.; Hirschfelder, J. O. *J. Chem. Phys.* **1959**, *30*, 1426.
(55) Hofacker, L. *Z. Naturforsch.* **1963**. *18a*, 607.
(56) Marcus, R. A. *J. Chem. Phys.* **1967**, *46*, 959.
(57) Truhlar, D. G. *J. Chem. Phys.* **1970**, *53*, 2041.
(58) Troe, J. In *Physical Chemistry: An Advanced Treatise, Vol. 6B*; Jost, W., Ed.; Academic: New York, 1975; p 835.
(59) Garrett, B. C.; Truhlar, D. G.; Grev, R. S.; Magnuson, A. W. *J. Phys. Chem.* **1980**, *84*, 1730.
(60) Villà, J.; Truhlar, D. G. *Theor. Chem. Acc.* **1997**, *97*, 317.
(61) (a) Nguyen, K. A.; Jackels, C. F.; Truhlar, D. G. *J. Chem. Phys.* **1996**, *104*, 6491. (b) Chuang Y.-Y.; Truhlar, D. G. *J. Phys. Chem.* **1998**, *102*, 242.
(62) Corchado, J. C.; Chuang, Y.-Y.; Fast, P.; Coitiño, E. L.; Hu, W.-P.; Liu, Y.-P.; Lynch, G. C.; Nguyen, K. A.; Jackels, C. F.; Gu, M. Z.; Rossi, I.; Clayton, S.; Melissas, V. S.; Steckler, R.; Garrett, B. C.; Isaacson, A. D.; Truhlar, D. G. POLYRATE-version 7.8, University of Minnesota, Minneapolis, MN 1997.
(63) (a) Gray, S. K.; Miller, W. H.; Yamaguchi, Y.; Schaefer, H. F. *J. Am. Chem. Soc.* **1981**, *103*, 1900. (b) Colwell, S. M. *Mol. Phys.* **1984**, *51*, 1217. (c) Colwell, S. M.; Handy, N. C. *J. Chem. Phys.* **1985**, *82*, 1281. (d) Nelson, H. H.; Adams, G. F.; Page, M. *J. Chem. Phys.* **1990**, *93*, 479. (e) Baldridge, K. K.; Gordon, M. S.; Steckler, R.; Truhlar, D. G. *J. Phys. Chem.* **1989**, *93*, 5107. (f) Garrett, B. C.; Koszykowski, M. L.; Melius, C. F.; Page, M. *J. Phys. Chem.* **1990**, *94*, 7096. (g) Truhlar, D. G.; Gordon, M. S. *Science* **1990**, *249*, 491. (h) González-Lafont, A.; Truong, T. N.; Truhlar, D. G. *J. Phys. Chem.* **1991**, *95*, 4618. (i) Liu, Y.-P.; Lynch, G. C.; Truong, T. N.; Lu, D.-h.; Truhlar, D. G.; Garrett, B. C. *J. Am. Chem. Soc.* **1993**, *115*, 2408. (j) Liu, Y.-P.; Lu, D.-h.; González-Lafont, A.; Truhlar, D. G.; Garrett, B. C. *J. Am. Chem. Soc.* **1993**, *115*, 7806.
(64) (a) Truhlar, D. G.; Isaacson, A. D.; Skodje, R. T.; Garrett, B. C. *J. Phys. Chem.* **1982**, *86*, 2252. (b) Tucker, S. C.; Truhlar, D. G. In *New Theoretical Concepts for Understanding Organic Reactions*; Bertrán, J., Csizmadia, I. G., Eds.; Kluwer Academic: Dordrecht, 1989; p 291.
(65) Lu, D.-h.; Truong, T. N.; Melissas, V. S.; Lynch, G. C.; Liu, Y.-P.; Garrett, B. C.; Steckler, R.; Isaacson, A. D.; Rai, S. N.; Hancock, G. C.; Lauderdale, J. G.; Joseph, T.; Truhlar, D. G. *Computer Phys. Commun.* **1992**, *71*, 235.
(66) Steckler, R.; Hu, W.-P.; Liu, Y.-P.; Lynch, G. C.; Garrett, B. C.; Isaacson, A. D.; Melissas, V. S.; Lu, D.-h.; Truong, T. N.; Rai, S. N.; Hancock, G. C.; Lauderdale, J. G.; Joseph, T.; Truhlar, D. G. *Computer Phys. Commun.* **1995**, *88*, 341.
(67) Steckler, R.; Chuang, Y.-Y.; Coitiño, E. L.; Hu, W.-P.; Liu, Y.-P.; Lynch, G. C.; Nguyen, K. A.; Jackels, C. F.; Gu, M. Z.; Rossi, I.; Fast, P.; Clayton, S.; Melissas, V. S.; Garrett, B. C.; Isaacson, A. D.; Truhlar, D. G. POLYRATE version 7.0, University of Minnesota, Minneapolis, MN, 1996.
(68) Truhlar, D. G.; *J. Comput. Chem.* **1991**, *12*, 266.
(69) Sears, T. J.; Johnson, P. M.; Jin, P.; Oatis, S. *J. Chem. Phys.* **1996**, *104*, 781.

Table 1. *Ab Initio* Geometries (Distances in Å and Angles in Degrees)[a]

		6-31G(*d*,*p*)		6-311G(*d*,*p*)			
	coordinate	HF	MP2	HF	MP2	CASSCF-(3,3)	QCISD-(T)
C_2H_4	R_{CC}	1.316	1.336	1.316	1.337	1.337	1.344
	R_{CH}	1.077	1.081	1.077	1.085	1.076	1.089
	Φ_{HCC}	121.7	121.6	121.7	121.7	121.6	121.5
SP[b]	R_{CC}	1.375	1.335	1.357	1.335	1.362	1.357
	R_1	2.009	1.864	1.983	1.869	1.880	1.967
	R_2	1.075	1.080	1.075	1.085	1.076	1.088
	R_3	1.076	1.080	1.076	1.084	1.075	1.088
	Φ	106.3	107.2	106.6	107.2	107.8	106.8
C_2H_5	R_{CC}	1.497	1.489	1.498	1.494	1.497	1.500
	R_1	1.086	1.089	1.086	1.094	1.086	1.098
	R_2	1.076	1.078	1.076	1.083	1.076	1.087
	R_3	1.091	1.095	1.091	1.100	1.114	1.104
	Φ	111.7	111.8	111.6	111.6	111.6	111.6

[a] Experimental values for C_2H_4: $R_{CC} = 1.339$ Å, $R_{CH} = 1.085$ Å, and $\Phi_{HCC} = 121.1$ (ref 70). [b] Saddle point.

Five-point Lagrange interpolation of the reaction-path data was used to obtain properties (geometry, energy, and generalized normal-mode frequencies) at every 0.00529 Å along the path from the saddle point to the equilibrium structures. The generalized free energy of activation was then calculated at each of these points, and the location of the variational transition state and the CVT rate constants (k_a^{CVT} and k_d^{CVT}) were determined by interpolating to the maximum of this function for each temperature. Frequencies between consecutive points along the reaction path were correlated adiabatically.[50,70]

Quantum mechanical tunneling effects were included by multiplying $k_a^{CVT}(T)$ and $k_d^{CVT}(T)$ by a transmission coefficient[50,53,59,64] $\kappa(T)$. As we will show later, the transition state occurs fairly early along the reaction path where the curvature of the reaction path is very small, and for this reason the zero-curvature tunneling (ZCT) semiclassical adiabatic ground-state approximation,[46,50,53,59,64] $\kappa^{CVT/ZCT}(T)$, has been employed. [Note that in our earlier papers the ZCT approximation is sometimes called the vibrationally adiabatic zero curvature (VAZC) approximation or the minimum-energy-path semiclassical adiabatic ground-state (MEPSAG) approximation.] The ZCT transmission coefficient is calculated as the Boltzmann average of the semiclassical probability, $P(E)$, of tunneling along the MEP through or over the ground-state vibrationally adiabatic potential barrier, $V_a^G(s)$, at energy E. The ZCT approximation is a multidimensional tunneling method because V_a^G includes the variation with s of the zero-point energy of all 14 vibrational modes that are orthogonal to the reaction coordinate.

Results

Geometries. The optimized geometries for the equilibrium and saddle point structures are presented in Table 1. The coordinates used in Table 1 are defined in Figure 1. The overall agreement among the various calculational methods is good, as is the agreement with previous calculations and experimental[71] values (where available). The carbon−carbon distance in ethylene is somewhat underestimated at the HF level, whereas the post-HF geometries have the C−C distance closer to the experimental distance of 1.339 Å. The same trends are observed for the carbon−hydrogen distance, with the exception of the CASSCF calculation, which does not improve the HF value.

(70) Villà, J.; González-Lafont, A.; Lluch, J. M.; Bertrán, J. *Mol. Phys.* **1996**, *89*, 633.

(71) Duncan, J. L. *Mol. Phys.* **1974**, *28*, 1177.

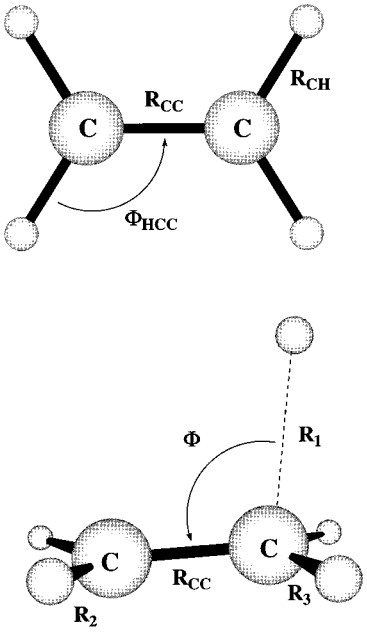

Figure 1. Definition of geometrical parameters for the C_2H_4 and C_2H_5 systems.

Even though the best calculation energywise is the QCISD(T) one, the MP2 optimized geometries are in better agreement with the experimental geometry. For ethyl radical, all methods reflect the expected lengthening of the carbon−carbon distance. In all the optimized geometries of C_2H_5, the R_1 and R_3 distances are clearly longer than that of R_2, which maintains the value it has in ethylene.

In the saddle point structures, the C_2H_4 moiety resembles ethylene. At the QCISD(T) level, the carbon−carbon distance is only 0.013 Å longer than in ethylene, and at the CASSCF and at HF levels, there is a greater increase. In contrast, at the MP2 level, the carbon−carbon distances have not changed from ethylene to the saddle point structure. The distance, R_1, for the attacking/departing hydrogen is 1.967 Å at the QCISD(T) level; the MP2 and CASSCF levels give smaller values for this distance (by ∼0.1 Å), whereas the HF R_1 distance is longer. Thus, the MP2 and CASSCF potential energy hypersurfaces have a saddle point structure that is more similar to the C_2H_5 system than is the saddle point of the QCISD(T) hypersurface. The bond angles are quite consistent across all levels of theory considered.

Energies and Reaction Path. Table 2 summarizes the results for the energetics of the $C_2H_4 + H \rightarrow C_2H_5$ reaction. (The last row of this table will be explained in the next section.)

The quantity ΔV is the classical energy of reaction; that is, the potential energy of the product of association, C_2H_5, relative to the potential energy of the reactants, $C_2H_4 + H$. The QCISD-(T)/B2//MP2/B1 and QCISD(T)/B2 values coincide, indicating that the geometric differences between MP2/B1 and QCISD-(T)/B2 minimum-energy structures are not energetically significant. The correction of spin contamination at the PMP2/B2//MP2/B1 level changes the MP2/B1 value of the reaction energy by 1.3 kcal/mol and provides an energy of reaction of −39.2 kcal/mol. This value in very good agreement with the QCISD(T)/B2 result, which is the highest level reported here. However, the CASSCF calculations underestimate the exoergicity by ∼8−9 kcal/mol. Because CASSCF includes internal (static) correlation energy, but a negligible portion of the external (dynamic) correlation energy, we conclude that the latter changes very appreciably over the course of reaction.

Table 2. Energetics (kcal/mol) for the $C_2H_4 + H \rightarrow C_2H_5$ Reaction[a]

method[b]	ΔV	$V^{\ddagger}$	$V^{\ddagger} - \Delta V$	ΔH_0	$\Delta H_0^{\ddagger}$	$\Delta H_0^{\ddagger} - \Delta H_0$
MP2/B1	−37.9	11.0	48.9	−32.0	12.7	44.7
PMP2/B1//MP2/B1	−39.2	3.1	42.3	−33.3		
CASSCF(3,3)/B2//MP2/B1	−30.7	8.5	39.1	−24.8		
CASSCF(3,3)/B2	−30.8	7.9	38.8	−24.9	9.4	34.3
QCISD(T)/B2//MP2/B1	−39.3	3.9	43.1	−33.4		
QCISD(T)/B2	−39.3	3.6	43.0	−33.4	3.8	37.2
PMP2/B1//MP2/B1///[c]	−39.2	4.0	43.2	−33.3	5.4	38.7
CASSCF(3,3)/B2//MP2/B1///[c]	−30.7	8.5	39.1	−24.8	10.3	35.1
QCISD(T)/B2//MP2/B1///[c]	−39.3	4.3	43.6	−33.4	5.7	39.1
VSEC//MP2/B1///[d]	−43.0	1.2	44.2	−37.1	2.7	39.8

[a] ΔV is the classical energy of reaction; $V^{\ddagger}$ is the classical barrier height; $V^{\ddagger} - \Delta V$ is the classical barrier height of the reverse reaction; ΔH_0 is the zero-point-inclusive energy of reaction, which equals the enthalpy of reaction at 0 K; $\Delta H_0^{\ddagger}$ is the zero-point-inclusive barrier height evaluated at the conventional transition state (saddle point); $\Delta H_0^{\ddagger} - \Delta H_0$ is the zero-point-inclusive barrier height for the reverse reaction evaluated at the saddle point. [b] B1: 6-31G(*d*,*p*); B2: 6-311G(*d*,*p*). [c] In the X//MP2/B1/// calculations, the $V^{\ddagger}$ and $\Delta H_0^{\ddagger}$ values correspond to carrying out high-level single-point energy calculations along the MP2/B1 reaction path and finding the maximum potential energy along the path. [d] See *Parameter Adjustment* section in text.

The quantity ΔH_0 is the 0 K heat of reaction. Our highest level calculation of this quantity is the QCISD(T) value, −33.4 kcal/mol. This theoretical value is 2 kcal/mol different from the best experimental result of -35.5 ± 1 kcal/mol, obtained by using the value[72] of 28.0 ± 1 kcal/mol for the 300 K C_2H_5 heat of formation. The discrepancy is understandable considering the small size of the B2 basis set, which has only a single set of polarization functions, although corrections for higher-level electron correlation effects could also be important.

The forward and reverse potential energy barriers, $V^{\ddagger}$ and $V^{\ddagger} - \Delta V$, evaluated in the usual ways (i.e., by geometry optimization of the saddle point and evaluation of the energy at the optimized structure), are the first six rows of Table 2. The approximate spin projection technique PMP2 lowers the MP2 addition and dissociation barriers by 6−8 kcal/mol. The PMP2 values are in fair agreement, 0.5−0.7 kcal/mol, with the QCISD(T)/B2 calculations, whereas the CASSCF calculations overestimate the addition barrier and underestimate the unimolecular dissociation barrier with respect to the QCISD(T)/B2 ones by ∼4−5 kcal/mol. Table 2 also gives the zero-point-inclusive barrier height for the forward reaction, $\Delta H_0^{\ddagger}$, and for the reverse reaction, $\Delta H_0^{\ddagger} - \Delta H_0$. These values are evaluated at the MP2/B1 saddle point location for rows 1, 2, 3, and 5, at the CASSCF(3,3)/B2 saddle point for row 4, and at the QCISD(T)/B2 saddle point for row 6.

Rows 7, 8, and 9 of Table 2 show the result of carrying out higher-level single-point calculations along the MP2/B1 reaction path and finding the maximum potential energy along the path. As already mentioned, a calculation involving single-point level-X calculations along a reaction path at level Y is called X//Y///. The deviations of these X//Y/// calculations from the most accurate result, QCISD(T)/B2, are comparable to the deviations found at the X//Y levels. The saddle point location is estimated by finding the highest X//Y/// energy along the path calculated at level Y. The maximum of the CASSCF/B2//MP2/B1/// potential energy curve is displaced toward C_2H_5, and the other two X//Y/// curves show a displacement of their maxima from the MP2/B1 saddle point structure toward the $C_2H_4 + H$ structure. The QCISD(T)/B2//MP2/B1/// forward classical barrier height, 4.3 kcal/mol, is only 0.7 kcal/mol higher than the QCISD(T)/B2 value calculated with full optimization. Despite the differing locations of the approximate saddle point geometries, the zero-point energies of the three X//Y/// saddle points are all in the range 34.3−34.6 kcal/mol. The zero-point energy difference between the maximum energy structure at the QCISD(T)/B2//MP2/B2/// level and the saddle point optimized at the QCISD(T)/B2 level is only 1.3 kcal/mol. These results and the geometries mentioned in the previous section suggest that, although it is inadequate from an energetic perspective, the MP2/B1 level may be useful for providing a reaction path that connects $C_2H_4 + H$ and C_2H_5. [When the maximum energy point of a series of single-point calculations along a reaction path does not agree well with full optimization of the saddle point at the higher level, which is often the case,[73] then the more complete VTST-IC version[74] of the /// approach (i.e., X///Y instead of X//Y///) may be preferred because in that approach the barrier height calculated by the full optimization is employed.]

Our highest-level unextrapolated result for the zero-point-inclusive barrier, $\Delta H_0^{\ddagger}$, is the full QCISD(T) result, 3.7 kcal/mol. The previous estimate of Hase et al.[29] is 2.7 kcal/mol.

If results in any of the first nine rows in Table 2 are used to calculate the rate constants for the title reaction, the computed values do not match the experimental results. At all levels, the computed $k_a^{\infty}(T)$ are too low relative to the experimental values. This result strongly implies that the calculated ab initio energy barriers for the addition reaction are too high. One strategy to fix this problem was suggested by Hase et al.,[29] who used the barrier height for $C_2H_4 + H$ addition as an adjustable parameter in conventional transition state theory calculations (including a transmission coefficient based on a one-dimensional Eckart tunneling approximation) to fit the experimental rate constants. We shall suggest an alternative way to proceed in the next section.

Parameter Adjustment. We now propose a new fitting procedure that allows both for a realistic shape of the reaction-path energy profile and also for the change in location of the variational transition state along the reaction path as a function of temperature. By using canonical variational transition state theory with semiclassical tunneling coefficients, we will fit the experimental k_a^{∞} and k_d^{∞} at the same time.

The basis of the new model is the Scaled External Correlation (SEC) method,[75,76] which is based on combining the results of two ab initio calculations: a CASSCF calculation that accounts for internal (or static) correlation effects and a multireference configuration interaction[77] (MRCI) that accounts for an ap-

(72) Castelhano, A. L.; Marriott, P. R.; Griller, D. *J. Am. Chem. Soc.* **1981**, *103*, 4262.

(73) (a) Espinosa-Garcia, J.; Corchado, J. C. *J. Phys. Chem.* **1995**, *99*, 8613. (b) Chuang, Y.-Y.; Truhlar, D. G., unpublished data.

(74) (a) W.-P. Hu, Y.-P. Liu, and D. G. Truhlar, *J. Chem. Soc., Faraday Trans.* **1994**, *90*, 1715. (b) Chuang, Y.-Y.; Truhlar, D. G. *J. Phys. Chem. A* **1997**, *101*, 6911.

(75) Brown, F. B.; Truhlar, D. G. *Chem. Phys. Lett.* **1985**, *117*, 307.

(76) Corchado, J. C.; Truhlar, D. G. *ACS Symp. Ser.*, in press.

preciable fraction of the external (or dynamical) correlation. Then, the accurate energy is approximated by:[75]

$$E_{\mathrm{SEC}} = E_{\mathrm{CASSCF}} + \frac{E_{\mathrm{MRCI}} - E_{\mathrm{CASSCF}}}{F} \tag{6}$$

where we assume that the nondynamical correlation is correctly introduced by the CASSCF term[78] and that the fraction of the dynamical correlation energy recovered by the MRCI calculation can be represented by a constant[75] or simple function F.

In the present paper we replace MRCI by QCISD(T). Although QCISD(T) is technically a single-reference method, it shares with coupled cluster methods a relative insensitivity to orbital basis,[79] and it has the major advantage over MRCI that it is size consistent.[45,80] Furthermore, the QCI approach is much less affected by spin contamination than the MP2 method. It has been shown previously that in the system under study, the QCISD(T) methodology yields similar energetic results to multireference configuration interaction methods,[29] while having the advantage of being computationally more convenient.

The major new feature introduced in the present paper is that in eq 6, F is assumed to be a function of geometry. In particular, we assume that F is a function of a distinguished coordinate that indicates the degree of advance of the reaction, which accounts for the fact that nondynamical correlation is not fully included in the QCISD(T) calculation as well as for the fact that the fraction of dynamical correlation energy recovered is not completely constant. To distinguish the new approach from the original SEC method[75,76] in which F was constant, we will call the new approach in which F is a function of geometry Variable Scaling of External Correlation (VSEC).

In the present application, the functional form of F is based on the bond energy-bond order (BEBO)[39,81,82] scheme, in which the bond order of a bond depends exponentially on distance, as originally postulated by Pauling.[83] Thus, we take

$$F = F_0 + F_1 \exp\left(-\frac{R_1 - R_{1,\mathrm{e}}}{\gamma}\right) \tag{7}$$

where F_0, F_1, and γ are adjustable parameters, R_1 is defined in Figure 1, and $R_{1,\mathrm{e}}$ is the R_1 distance at the MP2/B1 C_2H_5 equilibrium geometry ($R_{1,\mathrm{e}} = 1.095$ Å). In the present work, the three parameters were adjusted to reproduce as accurately as possible the high-pressure experimental rate constants for the addition and the unimolecular dissociation. This procedure allows us to get a consistent energy profile for studying the location and temperature dependence of the variational transition state of this reaction.

At the $C_2H_4 + H$ reactant (R) structure, R_1 is equal to infinity, yielding $F_{\mathrm{R}} = F_0$. Analogously, at the C_2H_5 product (P) structure, eq 7 reduces to $F_{\mathrm{P}} = F_0 + F_1$. Using these values yields

$$E^{\mathrm{P}}_{\mathrm{VSEC}} - E^{\mathrm{R}}_{\mathrm{VSEC}} = E^{\mathrm{P}}_{\mathrm{CASSCF}} - E^{\mathrm{R}}_{\mathrm{CASSCF}} + \frac{E^{\mathrm{P}}_{\mathrm{QCI}} - E^{\mathrm{P}}_{\mathrm{CASSCF}}}{F_0 + F_1} - \frac{E^{\mathrm{R}}_{\mathrm{QCI}} - E^{\mathrm{R}}_{\mathrm{CASSCF}}}{F_0} \tag{8}$$

where QCI is short for QCISD(T) in the present case. Note that the left-hand side of eq 8 is the VSEC approximation to the quantity called ΔV in Table 2.

To use eq 8, we require an estimate for ΔV, which is the classical energy difference between the C_2H_5 and $C_2H_4 + H$ systems. Ideally, this estimate would be available from a reliable ab initio calculation, but, as we have already pointed out, energy differences in radical addition reactions are very difficult to compute reliably, even if we use very high-level ab initio calculations. For this reason, we estimate ΔV by an iterative semiempirical method. A reasonable zeroth iterate for this energy difference is the value that is deduced from the transition state model of Hase et al.[29] In Table 5 of Hase et al.,[29] the authors used zero-point-inclusive barriers of 3.1 and 38.4 kcal/mol (the latter is the mean of all the values used) for the addition and the unimolecular dissociation, respectively. For the sake of consistency with our work, we calculate ΔV from these values by using ab initio frequencies instead of using the scaled values in Table 5 of Hase et al.[29] From the best ab initio frequency values of Table 2 in Hase et al.,[29] a ZPE increment between C_2H_4 and C_2H_5 of 5.6 kcal/mol is obtained. Combining these three values yields −40.9 kcal/mol as an estimate of ΔV. This classical energy value is used in eq 8 to provide a relation between F_0 and F_1; that is, for each trial value for F_0, a unique value of F_1 is calculated with eq 8. In this way, a table with all the allowed (F_0,F_1) pairs for a given classical energy difference is constructed.

From inspection of the table obtained as just described, (F_0,F_1) pairs with F_0 close to 1.0 and F_1 close to zero are selected. Such a choice of F_0 follows from the high level of the QCISD(T)/B2 calculation, and such a choice of F_1 is made because the dependence of the electron correlation with the bond distance, R_1, although not negligible, is probably small. For each of these (F_0,F_1) pairs, various values of the γ parameter are selected. For a set of three parameters, an energy profile is computed, and we perform a canonical variational transition state theory calculation with semiclassical multidimensional tunneling. We reject those sets of parameters that produce a variational displacement of the transition state out of the region where high level ab initio calculations have been carried out; namely, the range of R_1 distances from 1.793 to 2.171 Å. If we cannot obtain a good fit with the variational transition states in this range, we should extend the range.

Comparison with experimental values is done by applying Student's t test[84] to the rate constants values. If none of the trial sets give satisfactory results for the Student's t test, we change ΔV and repeat the process. This process is continued until good agreement with experiment is obtained.

After wide exploration, the parameters that were found to give theoretical rate constants close enough to experimental results (with a significance of 0.02 for Student's t test) were $F_0 = 1.1$, $F_1 = -0.0268$, and $\gamma = 3.846$ Å, with a classical energy difference for the addition process of $\Delta V = -43.0$ kcal/mol. Although $F_0 + F_1$ would ideally be <1, a value slightly >1 is acceptable in practical fitting. The maximum in the V_{MEP} curve obtained by the VSEC method (eqs 7 and 8) with that set of parameters is located at an s increment 0.148 Å earlier than

(77) Shavitt, I. In *Advanced Theories and Computational Approaches to the Electronic Structure of Molecules*; Dykstra, C. E., Ed.; Reidel: Boston, 1984; p 185.
(78) Mok, D. K. W.; Neumann, R.; Handy, N. C. *J. Phys. Chem*. **1996**, *100*, 6225.
(79) Lee, T. J.; Scuseria, G. E. In *Quantum Mechanical Electronic Structure Calculations with Chemical Accuracy*; Langhoff, S. R., Ed.; Kluwer: Dordrecht, 1995; p 47.
(80) Raghavachari, K.; Anderson, J. B. *J. Phys. Chem*. **1996**, *100*, 12960.
(81) Johnston, H. S.; Parr, C. A. *J. Am. Chem. Soc*. **1963**, *85*, 2544.
(82) Truhlar, D. G. *J. Am. Chem. Soc*. **1972**, *94*, 7584.
(83) Pauling, L. *J. Am. Chem. Soc*. **1947**, *69*, 542.
(84) Miller, J. C.; Miller, J. N. In *Statistics for Analytical Chemistry*, 2nd ed.; Ellis Horwood: London, 1988.

(looser than) the MP2/B1 saddle point location. This VSEC-estimated saddle point corresponds to $R_1 = 2.011$ Å, and the classical barrier height relative to the $C_2H_4 + H$ system is 1.2 kcal/mol. The bending frequencies of the forming bond at this location are 338 and 257 cm^{-1}. Including zero-point changes raises the forward classical barrier height from 1.2 kcal/mol to 2.7 kcal/mol, which is in excellent agreement with the value of Hase et al.[29] (It is worthwhile to note that our calculations were complete before the appearance of the erratum that lowered their value to 2.7 kcal/mol, so this is an independent determination.) The good agreement is encouraging from an empirical point of view because our method is quite different from theirs, involving variational transition state theory and a multidimensional tunneling approximation. Because our treatment is based on higher-level dynamical theory with less assumptions, it can give insight into the nature of the dynamical bottleneck, as discussed in the next section.

Our classical barrier heights for the forward and reverse reaction are 1.2 and 44.2 kcal/mol, respectively. The zero-point-inclusive barrier heights measured at the saddle point are 2.7 and 39.8 kcal/mol, respectively. However, because the saddle point is not the dynamical bottleneck and the variational transition becomes tighter as temperature increases, it is necessary to consider finite-temperature entropic effects as well as zero-point energy to get a correct physical model of the reaction. We shall see in the next section that it is necessary to consider more than just the reactants, product, and saddle point to model the dynamical bottlenecks for the thermal rate constants.

The energy of reaction and forward and reverse barrier heights as approximated by the VSEC method are given in the last row of Table 2. The value −37.1 kcal/mol that the VSEC treatment yields for ΔH_0, combined with a heat of formation of 12.548 kcal/mol[85] for ethylene at 298 K, implies a value of $\Delta H_{f,298} =$ 26.6 kcal/mol for the heat of formation of ethyl radical, which is in the range (25.8−28.8 kcal/mol) of experimental values,[20] but slightly lower than the values of 28.0−28.8 recommended by Hanning-Lee et al.[20] As noted by Hase et al.,[29] the data available for the reverse reaction are not discriminating enough to predict reliable values for ΔV and the heat of formation of the products. In this light, the prediction of the product heat of formation within 1.5 kcal/mol is acceptable confirmation that our reaction path model is globally realistic. In the next section we concentrate on the bottleneck properties on the reactant side of the reaction path and tunneling through the barrier region, which are the central points of this study.

Dynamics. The final calculated values of k_a^∞ and k_d^∞ are given in Arrhenius form in Figures 2 and 3, respectively, along with the experimental results. Dotted lines represent the CVT results and solid lines stand for CVT/ZCT results. Figure 2 shows some dispersion in the oldest values at 298 K, probably due to the extrapolations from low-pressure results that were necessary to obtain estimates of the high-pressure-limit rate constants. Notice that the two figures cover different temperature ranges.

Figure 2 shows that tunneling is important for temperatures below ∼500 K. The ZCT transmission coefficient is 1.14, 1.23, 1.44, and 2.37 at 500, 400, 300, and 200 K, respectively. If tunneling is neglected, the deviation from experimental values is a factor of 1.6 and 2.8 at temperatures of 300 and 200 K, respectively, with a factor of 2.1 discrepancy at 250 K. Figure 2 illustrates very dramatically that the widely discussed curvature

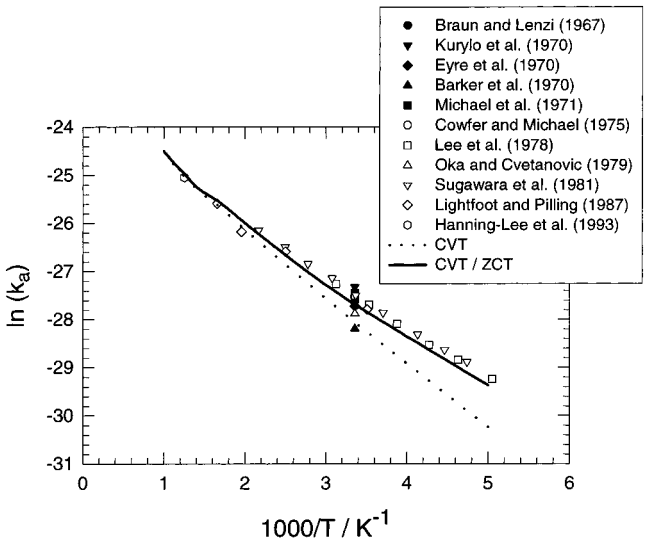

Figure 2. Arrhenius plot for the high-pressure limit of the addition rate constant, k_a^∞. The solid and dotted lines are the calculated rate constants with and without tunneling, respectively, and the symbols are experimental results.[4,6−11,12,14,17,20]

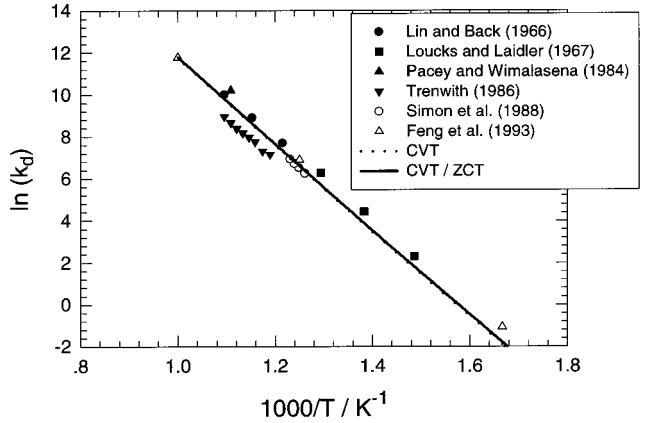

Figure 3. Arrhenius plot for the high-pressure limit of the unimolecular dissociation rate constant, k_d^∞. The solid and dotted lines are the calculated rate constants with and without tunneling, respectively, and the symbols are experimental results.[3,15,16,18,21] Note that the dotted line is practically hidden by the solid line.

of the Arrhenius plot for this addition reaction is almost entirely due to tunneling. Thus, the CVT calculation without tunneling yields nearly a straight line in Figure 2, whereas the nonlinear CVT/ZCT curve incorporating the VSEC multidimensional tunneling contribution tracks the experimental results rather faithfully. Although it was concluded even in early work that the temperature dependence of the partition coefficients was probably insufficient to account for the temperature dependence of the rate constants, only relatively crude tunneling calculations were available.[1,2]

Figure 3 shows a somewhat greater dispersion in the experimental values, and Trenwith's results[15] are significantly different from the rest. Inclusion of the semiclassical tunneling coefficient in the calculation is now less important because all the experimental values were obtained at high temperatures (600 K and higher); the ZCT transmission coefficient decreases from 1.09 at 600 K to 1.03 at 1000 K.

In Table 3 we present the properties corresponding to the variational transition states at several temperatures. In the second column of this table the displacements of the transition state with respect to the VSEC saddle point geometry are

(85) Lide, D. R., Ed.; *Handbook of Chemistry and Physics*, 76th ed.; CRC: Boca Raton, FL, p 5-4.

Table 3. Properties Corresponding to the VSEC Variational Transition State at Several Temperatures

T(K)	s(Å)[a]	R_1 (Å)[b]	$V_{MEP} - \Delta V$[c]	freq (cm^{-1})[d]	$\Delta G_a^{CVT,0}$[e]	$\Delta G_d^{CVT,0}$[f]
200	0.057	1.954	44.1	395, 335	2.4	39.8
300	0.078	1.932	44.1	417, 365	2.4	39.9
400	0.088	1.923	44.0	427, 379	2.5	40.0
500	0.095	1.916	44.0	435, 389	2.7	40.1
600	0.106	1.905	44.0	447, 405	2.7	40.2
700	0.144	1.868	43.7	488, 460	2.9	40.4
800	0.146	1.867	43.7	490, 463	3.1	40.5
900	0.147	1.865	43.7	492, 465	3.2	40.7
1000	0.149	1.864	43.7	494, 467	3.4	40.9

[a] Relative to the VSEC saddle point. [b] See Figure 1. [c] Potential energy relative to C_2H_5, in kcal/mol. [d] The two H...C = C bending frequencies about the rupturing bond. [e] CVT standard-state free energy of activation, in kcal/mol. [f] CVT standard-state free energy of activation, in kcal/mol.

presented. Negative values of s correspond to the $C_2H_4 + H$ side of the saddle point. Note that the variational transition state is tighter than the saddle point. This is expected[39] for an early saddle point in an exothermic reaction because the variational effect is controlled by the tightening of transitional bending modes; that is, bending modes whose frequencies vanish asymptotically. Furthermore, the variational transition state becomes tighter (moves toward the C_2H_5 product) as the temperature increases, also in accord with previous variational transition state theory results.[34,39,86−93] The maximum of the VSEC vibrationally adiabatic ground-state potential curve V_a^G, which is the maximum of the standard-state generalized transition state theory free energy of activation profile[39,48] at 0 K, also appears at positive s ($s = 0.039$ Å), corresponding to a geometry where R_1 is 1.971 Å. The movement of the variational transition state from $s = 0.039$ Å at 0 K to $s = 0.149$ Å at 1000 K corresponds to shortening of ∼0.11 Å in the R_1 distance, with a concomitant change of 0.4 kcal/mol in V_{MEP} at the variational transition state. The V_a^G curve is rather flat in this region, dropping 0.3 kcal/mol from the saddle point value, but finite-temperature entropic effects are more important. The only generalized normal-mode frequencies that suffer important changes in the region that contains the variational transition states at the different temperatures are the C−C stretching and the two H−C−C bending frequencies about the forming bond. Values of these bending frequencies at the variational transition states are shown in column 5 of Table 3. These low frequencies have an important weight in the entropic term[34,39,70,85] of the CVT free energy of activation (last two columns of Table 3), and they have provoked considerable discussion in the literature concerning their loose or tight character. As shown in Table 3, as temperature increases from 200 to 1000 K, these two bending frequencies at the variational transition state increase by 99 and 132 cm^{-1}, respectively. However, even at 1000 K, the variational transition state calculated here is looser than the one calculated by Hase et al.,[27] which has bending frequencies of 399 and 369 cm^{-1}, or by Hase et al.,[29] values of 422 and 382 cm^{-1} for the same frequencies. Thus, our study does not support the conclusions of Feng et al.[21] (namely, that a tighter transition state than that used by Hase and Schlegel[25,26] is required for a good fit to the temperature dependence of the experimental k_d^∞).

The bending frequencies at the 200 K dynamical bottleneck are 17% and 30% larger than at the VSEC saddle point, and the bending frequencies at 1000 K are factors of 1.5 and 1.8 larger than at the VSEC saddle point. These ratios show that a proper understanding of association reactions cannot be based on calculations only at the saddle point; entropic bending effects that tend to tighten the dynamical bottleneck location are important, and they compete successful with energetic effects in determining that location, with the effect being quite large at 1000 K. Nevertheless, these effects can be estimated using the present direct dynamics scheme based on variable scaling of external correlation energy.

Summary and Concluding Remarks

We have introduced a new method, VSEC (variable scaling of external correlation), for extrapolating electronic structure calculations to the limit of full configuration interaction and a complete one-electron basis set. The VSEC method assumes that separate estimates are available for the nondynamical and total correlation energies, and that the fraction of correlation energy recovered is a smooth function of geometry. In the present application, that smooth function is taken as a monotonic function of a single internal coordinate corresponding to the breaking bond. The assumption that a single internal coordinate is appropriate is justified by the fact that radical addition reactions satisfy the Bell-Evans-Polanyi principle.[94a] According to this principle, if no bonding elements occur in the transition state that do not also occur in either the reactants or products, the delocalization energy correlates monotonically with a single reaction coordinate.[94b] It will be interesting in future work to explore the applicability of the VSEC model for other reaction types.

One of the principal advantages of the VSEC model is that it does not presume a particular shape or even a functional form for the reaction barrier. By parametrizing the fraction of dynamical correlation energy recovered rather than parametrizing the potential energy hypersurface, we allow an arbitrary shape of the reaction path energy profile. This factor is particularly important for the credibility of tunneling calculations.

We have employed variational transition state theory in which the dynamical bottleneck is equated to the variational transition state, which in turn is identified with the structure with the maximum free energy of activation for both the forward and reverse reaction. The variational displacement of the dynamical bottleneck from the location of the saddle point depends on temperature, and in the range of temperatures from 200 and 1000 K, it ranges from 0.06 to 0.15 Å, with the variational transition state being tighter than the saddle point. The potential energy varies by only ∼0.4 kcal/mol over the range of geometries where the dynamical bottlenecks are found, but the C−C−H bend frequencies are 156 and 210 cm^{-1} higher at the 1000 K variational transition state than at the saddle point location and >100 cm^{-1} higher than at the 200 K variational transition state. Because these changes with temperature correspond to 25−40% increases in the bend frequencies, it means we must be very cautious about interpreting addition reactions in terms of a temperature-independent transition state. The fact that the frequencies at the variational transition states differ from the saddle-point frequencies means that converging

(86) Hase, W. L. *J. Chem. Phys.* **1976**, *64*, 2442.
(87) Quack, M.; Troe, J. *Ber. Bunsen-Ges. Phys. Chem.* **1977**, *81*, 329.
(88) Rai, S. N.; Truhlar, D. G. *J. Chem. Phys.* **1983**, *79*, 6046.
(89) Hase, W. L. *Accounts Chem. Res.* **1983**, *16*, 258.
(90) Hu, X.; Hase, W. L. *J. Phys. Chem.* **1989**, *93*, 6029.
(91) Hase, W. L.; Wardlaw, D. M. *Adv. Gas-Phase Photochem. Kinet.* **1989**, 2, 171.
(92) Klippenstein, S. J.; Marcus, R. A. *J. Chem. Phys.* **1990**, *93*, 2418.
(93) Wardlaw, D. M.; Marcus, R. A. *Adv. Chem. Phys.* **1987**, *70*, 231.
(94) Dewar, M. J. S.; Dougherty, R. C. *The PMO Theory of Organic Chemistry*; Plenum: New York, 1975; (a) p 310, (b) pp 219−220.

electronic structure calculations for stationary-point energies and geometries is only a first step at providing true understanding of the dynamics, even if the goal is simply to understand thermal high-pressure-limiting rate constants. Nevertheless fully characterizing the saddle point is an important first step, and one that still eludes us in a fully ab initio sense. Thus, we should remember that the present results are based on an electronic structure extrapolation method that, although suggestive and qualitatively stimulating, is surely susceptible to quantitative improvement.

Because the transition state occurs fairly early along the reaction path, tunneling was estimated by a zero-reaction-path-curvature scheme. The variation of zero-point energies along the tunneling path was included for all 14 transverse vibrational modes. Tunneling is found to be important for temperatures $<\sim$500 K, increasing the calculated rate constants by 23, 44, and 137% at 400, 300, and 200 K respectively, and accounting for the lion's share of the curvature observed in Arrhenius plots.

Acknowledgment. This work was supported in part by the U. S. Department of Energy, Office of Basic Energy Sciences. Financial support from DGES (project No. PB95-0637) and the use of the computational facilities of the "Centre de Computació i de Comunicacions de Catalunya" are gratefully acknowledged.

JA980131O